Contribution from the Departments of Chemistry, State University of New York at Buffalo, Buffalo, New York 14214, and Florida International University, Miami, Florida 33199

Electron Density Studies of Porphyrins and Phthalocyanines. 7. Electronic Ground State of Bis(pyridine)(*meso*-tetraphenylporphinato)iron(II)

Naiyin Li,[†] Philip Coppens,*[†] and John Landrum[‡]

Received June 16, 1987

The structure and electron density distribution of bis(pyridine)(*meso*-tetraphenylporphinato)iron(II), $FeN_6C_{54}H_{38}$, have been determined by using two sets of X-ray diffraction data collected at 110–120 K. Crystal data: M_r = 826.79, triclinic, $P\bar{1}$, Z = 1, a = 9.423 (1) Å, b = 10.560 (2) Å, c = 11.998 (2) Å, α = 101.70 (1)°, β = 104.96 (1)°, γ = 111.95 (2)°, V = 1008.50 (2) Å^3, d_{calcd} = 1.361 g/cm^3, μ = 4.17 cm^{-1}, λ(Mo Kα) = 0.71073 Å. R factors of the final aspherical atom refinements: R = 2.44%, R_w = 2.41% for data set 1 [$(\sin\theta)/\lambda_{max}$ = 0.91 Å^{-1}]; R = 3.98%, R_w = 2.85% for data set 2 [$(\sin\theta)/\lambda_{max}$ = 1.15 Å^{-1}]. The Fe–N(pyridine) distance is 2.037 (2) Å, while the average Fe–N(porphinato) distance is 2.001 (1) Å. Bond lengths and electron density distribution indicate that the iron atom is in the low-spin state. The experimental populations of the iron d orbitals are close to those from an extended Hückel calculation, with significant population of the crystal field destabilized orbitals, indicating σ-donation from the coordinated ligands. Covalency parameters derived from the $d_{x^2-y^2}$ populations in three complexes correlate with bond lengths. π-Back-bonding is suggested by the less-than-six total electron population of the d_{xz}, d_{yz}, and d_{xy} orbitals. The calculated Mössbauer shift is equal within experimental error to the spectroscopically observed value and has a negative sign.

Introduction

A full understanding of the biological action of heme proteins requires a detailed knowledge of the electronic structure of the prosthetic heme group, which is modeled by metal porphyrin compounds.[1] The electronic structure of metal porphyrins has received extensive attention.[2] Nevertheless, many unresolved issues remain, in part because the close spacing of the metal porphyrin energy levels requires a precise estimate of the effect of configuration interaction before even the nature of the ground state can be established in some of the complexes.[3] We have established in previous studies[4-9] that the electron density in molecules as large as the porphyrins can be mapped by using accurate X-ray diffraction data. The iron complexes studied included two four-coordinate intermediate-spin Fe(II) compounds,[5,6] a five-coordinate high-spin Fe(III) complex,[7] and two six-coordinate high-spin compounds, one each with Fe(II) and Fe(III).[8,9] To complete this series we present here a study of a six-coordinate low-spin Fe(II) complex. Further studies in this series will concentrate on small-molecule (O_2, NO, CO, and H_2O) adducts of iron porphyrins.

Experimental Section

Sample Preparation. All manipulations were carried out in a Vacuum/Atmospheres glovebox. Solvents were distilled from Na/benzophenone (toluene) and NaOH (pyridine) and stored sealed in the glovebox prior to use. Pyridine was stored over freshly activated molecular sieves. A 100-mg sample of Fe(TPP)[10] was dissolved in a minimal volume of refluxing toluene to which 1–2 mL of pyridine was added. The reaction mixture was filtered hot, and suitable single crystals were isolated in good yield upon cooling.

Data Collection. X-ray intensity data were measured by θ–2θ scans on a CAD4 diffractometer using graphite-monochromated Mo Kα radiation (50 kV, 20 mA), and a stream of cold nitrogen gas was used to cool the crystal. Two sets of data were collected. For the first set, collected at 120 ± 5 K, a 0.23 × 0.23 × 0.15 mm dark purple, capillary-sealed crystal was used. A total of 10874 reflections with $(\sin\theta)/\lambda < 0.81$ Å^{-1} ($\theta < 35°$) were collected. After solution of the structure with these data, high-order reflections were calculated, and only reflections calculated to have significant intensity were measured beyond 0.81 Å^{-1}. The crystal was lost during delivery of a nitrogen replacement tank after data up to $(\sin\theta)/\lambda$ = 0.91 Å^{-1} had been collected. A second crystal, with dimensions 0.16 × 0.16 × 0.14 mm, was used to collect 17151 reflections with 0.05 Å^{-1} < $(\sin\theta)/\lambda$ < 1.15 Å^{-1} at 110 ± 5 K. High-order reflections were again selected by calculation. Unit cell dimensions were obtained by a least-squares fit to the Kα_1 peaks of 25 centered reflections of crystal 2 with 24.8° < θ < 48.2°. Crystal data and experimental details are summarized in Table I.

Data Reduction. The reflection profiles were analyzed as described by Blessing.[11] The intensities of the standard reflections were fitted to cubic polynomials, which were used for scaling of the data. Corrections were made for absorption by the crystal and capillary[12,13] and for inhomogeneity for the incident beam. Ranges of the various corrections are

Table I. Experimental Data for $FeTPP(py)_2$

	crystal 1	crystal 2
space group	$P\bar{1}$	
temp, K	120 (5)	110 (5)
cell dimens		
a, Å		9.423 (1)
b, Å		10.560 (2)
c, Å		11.998 (2)
α, deg		101.70 (1)
β, deg		104.96 (2)
γ, deg		111.95 (2)
V, Å^3		1008.50 (2)
Z	1	
d_{calcd}, g/cm^3	1.361	
abs coeff, cm^{-1}	4.17	
cryst dimens, mm	0.23 × 0.23 × 0.15	0.16 × 0.16 × 0.14
mounted approx parallel to capillary	a^*	a^*
diam, mm	0.3	0.2
wall thickness, mm	0.02	0.02
abs coeff, mm^{-1}	1.058	1.058
radiation	Mo Kα; λ = 0.7107 Å	
scan type	θ–2θ	
scan width, deg	1.5 + 0.525 tan θ	
scan speed, deg/min	0.4–3.4	
θ(min)–θ(max), deg	0.04–35	0.04–55
$(\sin\theta)/\lambda_{min}$–$(\sin\theta)/\lambda_{max}$, Å^{-1}	0.05–0.90	0.05–1.15
hkl; lower limit–upper limit	$\bar{1}5,\bar{1}8,0$–14,16,21	$\bar{2}1,\bar{2}3,0$–20,23,27
time period, h	576	1136
no. of std reflcns	4 ($\bar{6}4\bar{1}$; 3,$\bar{4}$,10; $\bar{1}\bar{6}6$; $\bar{3}$,7,$\bar{1}\bar{2}$)	
no. of reflcns measd	10874	17151
no. of symm-indep reflcns	8942	12899
no. of $F > 6\sigma(F)$ reflcns	5672	8497

Table II. Data Averaging

	crystal 1	crystal 2
no. of reflcns measd	10874	17151
no. of symm-related and repeated reflcns	2423	5969
agreement factor $R = \sum\|I - \bar{I}\|/\sum I$	0.0191	0.0148
no. of symm-indep reflcns	8942	12899

[†] State University of New York at Buffalo.
[‡] Florida International University.

(1) Suslick, K. S.; Reinert, T. J. *J. Chem. Ed.* **1985**, *62*, 974–983. Jones, R. D.; Summerville, D. A.; Basolo, F. *Chem. Rev.* **1979**, *79*, 139–179.
(2) Loew, G. H. In *Iron Porphyrins*; Lever, A. B. P., Gray, H. B., Eds.; Addison-Wesley: Reading, MA, 1983; Part 1.
(3) Edwards, D. W.; Weiner, B.; Zerner, M. C. *J. Am. Chem. Soc.* **1986**, *108*, 2196–2204.

0020-1669/88/1327-0482$01.50/0

Table III. Summary of Least-Squares Refinements for Crystal 1

	I	II	III	IV
description	spherical atom, all data	spherical atom, high order	spherical atom, low order	multipole refinement
(sin θ)/λ range, Å^{-1}	0.05–0.91	0.70–0.91	0.05–0.70	0.05–0.91
no. of observns	5758	1553	4205	5758
no. of variables	353	333[a]	333[a]	478
$R(F)$, %	3.75	3.76	3.68	2.44
$R_w(F)$, %	3.98	3.71	4.15	2.41
$R(F^2)$, %	5.99	6.0	6.12	3.41
$R_w(F^2)$, %	7.79	7.1	8.15	4.66
GOF	1.69	1.06	1.97	1.03
scale factor	0.406 (2)	fixed to be 0.406		0.402 (1)

[a] H temperature factors and scale factor not refined.

Table IV. Summary of Least-Squares Refinements for Crystal 2

	I	II	III	IV
description	spherical atom, all data	spherical atom, high order	spherical atom, low order	multipole refinement
(sin θ)/λ range, Å^{-1}	0.05–1.15	0.70–1.15	0.05–0.70	0.05–1.15
no. of observns	8497	4530	3967	8497
no. of variables	353	333[a]	333[a]	478
$R(F)$, %	5.24	6.81	3.69	3.98
$R_w(F)$, %	4.23	6.71	3.84	2.85
$R(F^2)$, %	7.26	11.60	5.77	4.91
$R_w(F^2)$, %	8.26	13.26	7.54	5.61
GOF	1.50	1.10	1.93	1.02
scale factor	0.277 (2)	fixed to be 0.277		0.2675 (7)

[a] H temperature factors and scale factor not refined.

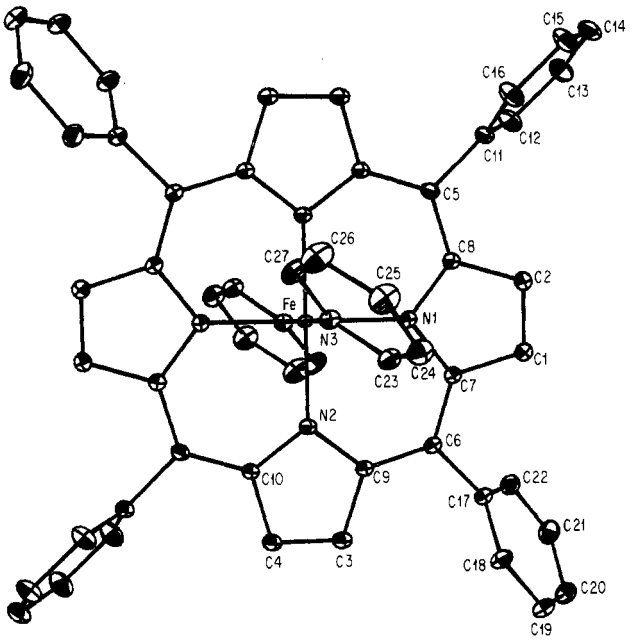

Figure 1. ORTEP drawing of the molecule indicating atom numbering. Ellipsoids are 50% probability surfaces. The Fe atom is located at a center of symmetry.

listed in the supplementary material. Agreement factors from the averaging of equivalent reflections are given in Table II.

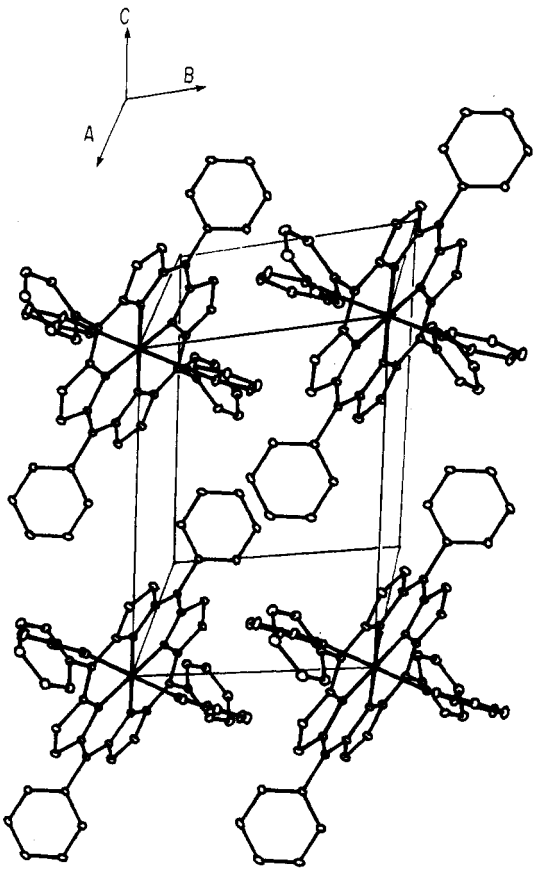

Figure 2. ORTEP drawing of the molecular packing. Ellipsoids are 50% probability surfaces.

Structure Analysis and Multipole Refinement

Positions of Fe, N, and C atoms were obtained from Patterson and Fourier maps. H atoms subsequently were located by difference Fourier methods. All least-squares refinements minimized the function $\sum w(F_o - K\|F_c\|)^2$, where $w = 1/\sigma^2(F) = 4F^2/\sigma^2(F^2)$; $\sigma^2(F^2) = PF^2 + \sigma_{counting}{}^2(F^2)$. The instrumental instability factor P was estimated from errors in the

(4) Stevens, E. D. *J. Am. Chem. Soc.* **1981**, *103*, 5087–5095.
(5) Lecomte, C.; Chadwick, D. L.; Coppens, P.; Stevens, E. D. *Inorg. Chem.* **1983**, *22*, 2982–2992.
(6) Coppens, P.; Li, L. *J. Chem. Phys.* **1984**, *81*, 1983–1993.
(7) Tanaka, K.; Elkaim, E.; Liang, L.; Zhu, N. J.; Coppens, P.; Landrum, J. *J. Chem. Phys.* **1986**, *84*, 6969–6978.
(8) Lecomte, C.; Blessing, R. H.; Coppens, P.; Tabard, A. *J. Am. Chem. Soc.* **1986**, *108*, 6942–6950.
(9) Elkaim, E.; Tanaka, K.; Coppens, P.; Scheidt, W. R. *Acta Crystallogr., Sect. B: Struct. Sci.* **1987**, *B43*, 457–461.
(10) Collman, J. P.; Hoard, J. L.; Kim, N.; Lang, G.; Reed, C. A. *J. Am. Chem. Soc.* **1975**, *97*, 2676–2681.
(11) Blessing, R. H. *J. Appl. Cryst.* **1986**, *19*, 412.
(12) Coppens, P.; Leiserowitz, L.; Rabinovitch, D. *Acta Crystallogr.* **1965**, *18*, 585.
(13) DeTitta, G. *J. Appl. Cryst.* **1985**, *18*, 75–79.

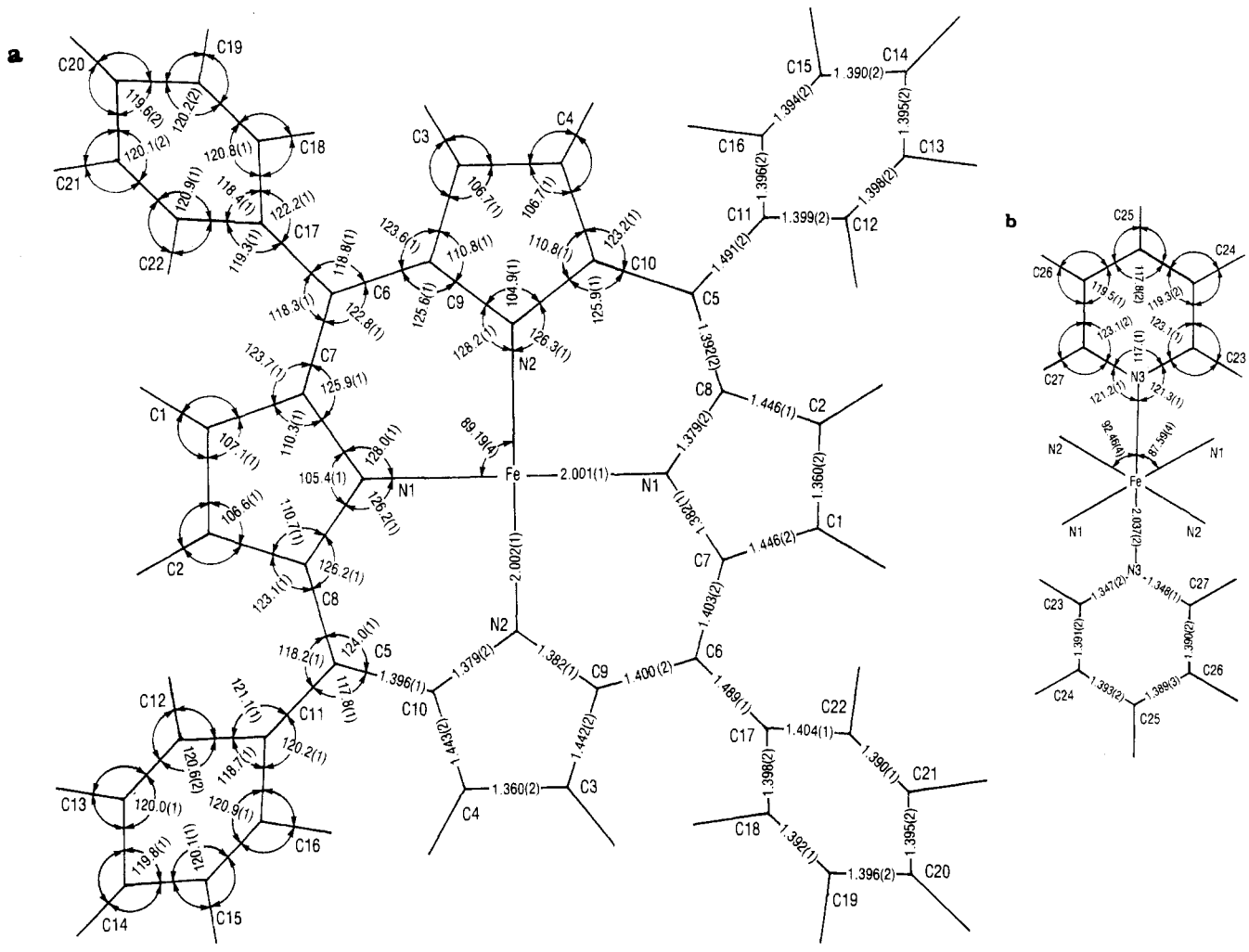

Figure 3. (a) Bond lengths and angles: (a) for non-hydrogen atoms in the Fe tetraphenylporphyrin moiety; (b) for non-hydrogen atoms involving the axial ligands.

time-dependent scaling polynomials and the fluctuations of the standards,[11] to be 0.0144 and 0.0118 for crystals 1 and 2, respectively.

Anisotropic temperature parameters were applied to all non-H atoms. Four different refinements for each data set are summarized in Tables III and IV. They include all-data, low-order and high-order spherical atom and all-data aspherical atom refinements. Neutral-atom scattering factors of Fe, N, C, and H, were taken from ref 14. ORTEP drawings[15] of the molecule and a packing diagram are shown in Figures 1 and 2.

In the aspherical atom multipole refinements[16,17] the electron density at each atom is described by an expansion of atom-centered deformation functions:

$$\rho_{atom}(r) = \rho_{core}(r) + \kappa^3 P_{val}\rho_{val}(\kappa r) + \sum_{l=0}^{l=4} \kappa'^3 R_l(\kappa' r) \sum_{m=0}^{l} P_{lm\pm} y_{lm\pm}$$

where ρ_{core} and ρ_{val} are spherical Hartree–Fock core and valence densities and κ and κ' are expansion–contraction parameters, which can be refined along with the populations P_{val} and $P_{lm\pm}$. R_l and $y_{lm\pm}$ are the radial and the real spherical harmonic functions, respectively. The third term accounts for the aspherical deformation of the valence electron density due to the formation of the chemical bonds and the accumulation of density in the lone-pair regions. For nitrogen, carbon, and hydrogen atoms, Slater-type radial functions of the form $R_l(\kappa' r) = Nr^{n_l} \exp(-\kappa' \zeta r)$ were used for the multipole deformation functions. Here N is a normalization parameter, and n_l and ζ, selected as described elsewhere,[17] are given in the supplementary material. For the iron atom, Hartree–Fock radial functions modified by the κ' parameter, rather than Slater-type functions, were used for the multipole deformation functions, to reflect the fact that the asymmetry around iron is essentially due to different occupancies of d orbitals. The same functions should therefore be used for both the monopoles and multipoles on the Fe atom. The corresponding Fourier–Bessel transforms $\langle j_0 \rangle$, $\langle j_2 \rangle$, and $\langle j_4 \rangle$ are given in ref 14.

To reduce the number of charge density parameters, the populations of chemically equivalent atoms were constrained to be equal. These constraints are justified a posteriori by the lack of major features in the residual density maps calculated after the final least-squares cycles. Since neither preliminary aspherical refinements nor deformation density maps showed significant deviations from D_{4h} symmetry around the iron, the iron atom was assumed to have this symmetry. Symmetry constraints for other atoms are given in the supplementary material, as are the atomic coordinate systems (Figure S1).

The multipole expansion was truncated at the hexadecapolar level ($l = 4$) for iron and at the octapolar level ($l = 3$) for the nitrogen and carbon atoms. The angular deformation of the hydrogen atom was described by a single dipole along the C–H axis.

As the crystal 2 data set is more complete, we will concentrate in the discussion below on these results except where necessary to illustrate the consistency between the two independent experiments. Fractional coordinates and temperature factors are listed in Tables V and S4 (supplementary material), respectively, while the bond lengths and angles involving non-hydrogen atoms from the final multipole refinement are given in Figure 3. Information on the hydrogen atoms is listed in the supplementary material. Population parameters for both sets of data of crystals 1 and 2 are given in the supplementary material. A residual map, calculated after completion of the multipole refinement, is shown in Figure 4. A residual feature along the Fe–N_2 bond is observed, which may be an indication of a slight orthorhombicity of the iron environment. Figures 5–7 show the deformation density maps. They represent the difference between the densities calculated from the observed structure factors and calculated phases and from the structure factors calculated

(14) *International Tables for X-ray Crystallography*; Kynoch: Birmingham, England, 1974; Vol. 4.
(15) Johnson, C. K. Report ORNL-5138; Oak Ridge National Laboratory: Oak Ridge, TN, 1976.
(16) Coppens, P. In *Electron Distributions and the Chemical Bond*; Coppens, P., Hall, M. B., Eds.; Plenum: New York, NY, 1982.
(17) Hansen, N. K.; Coppens, P. *Acta Crystallogr., Sect. A: Cryst. Phys., Diffr., Theor. Gen. Crystallogr.* **1978**, *A34*, 909–921.

Table V. Positional Parameters and Their Estimated Standard Deviations (Crystal 2, Multipole Refinement)

atom	x	y	z
Fe	0.0000	0.0000	0.0000
N_1	0.2249 (1)	0.09831 (9)	−0.00424 (7)
N_2	0.1010 (1)	−0.02153 (8)	0.15928 (9)
N_3	0.02736 (9)	0.2001 (2)	0.08453 (9)
C_1	0.5082 (1)	0.2178 (1)	0.0511 (1)
C_2	0.4401 (1)	0.2360 (1)	−0.05533 (9)
C_3	0.2831 (1)	−0.0384 (1)	0.3214 (1)
C_4	0.1295 (1)	−0.1110 (1)	0.3211 (1)
C_5	0.1527 (1)	0.1633 (1)	−0.19045 (9)
C_6	0.3963 (1)	0.0952 (1)	0.18964 (9)
C_7	0.3741 (1)	0.1315 (1)	0.08242 (9)
C_8	0.2638 (1)	0.1628 (1)	−0.08844 (9)
C_9	0.2647 (1)	0.0177 (1)	0.22128 (9)
C_{10}	0.0174 (1)	−0.0990 (1)	0.22100 (9)
C_{11}	0.2194 (1)	0.2408 (1)	−0.27016 (9)
C_{12}	0.2052 (1)	0.1646 (1)	−0.3856 (1)
C_{13}	0.2651 (1)	0.2385 (1)	−0.4607 (1)
C_{14}	0.3399 (1)	0.3896 (1)	−0.4204 (1)
C_{15}	0.3569 (1)	0.4661 (1)	−0.3050 (1)
C_{16}	0.2967 (1)	0.3920 (1)	−0.2306 (1)
C_{17}	0.5672 (1)	0.1507 (1)	0.27746 (9)
C_{18}	0.6855 (1)	0.1209 (1)	0.2433 (1)
C_{19}	0.8485 (1)	0.1862 (1)	0.3238 (1)
C_{20}	0.8961 (2)	0.2832 (1)	0.4399 (1)
C_{21}	0.7784 (2)	0.3108 (1)	0.4763 (1)
C_{22}	0.6154 (1)	0.2442 (1)	0.3962 (1)
C_{23}	−0.0893 (2)	0.2421 (1)	0.0442 (1)
C_{24}	−0.0657 (2)	0.3838 (2)	0.0868 (1)
C_{25}	0.0837 (2)	0.4883 (2)	0.1770 (1)
C_{26}	0.2025 (2)	0.4447 (2)	0.2218 (1)
C_{27}	0.1702 (2)	0.3012 (2)	0.1739 (1)

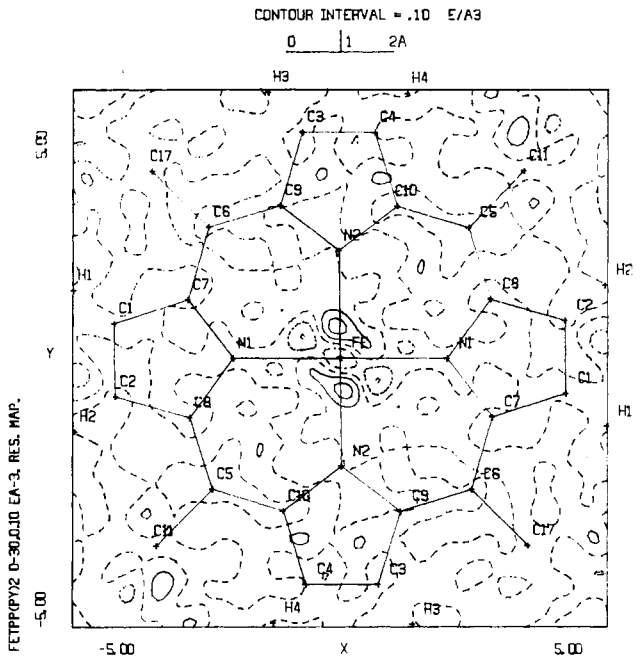

Figure 4. Residual map in the plane of the porphyrin ring. Contour interval = 0.1 e Å^{-3}. Zero and negative contours are broken.

with spherical atom form factors and the final parameters from the multipole refinement:

$$\Delta\rho(r) = \frac{2}{V}\sum_{H=0}^{H_{max}}\left(\frac{F_o}{\kappa} - F_c\right)\exp(-2\pi i H\cdot r)$$

Results and Discussion

Description of the Molecular Structure. The bond lengths of Fe–N_1, Fe–N_2, and Fe–N_3 are 2.001 (1), 2.002 (1), and 2.037 (1) Å, respectively, as compared with 1.989 (1), 1.997 (1), and 2.039 (1) Å in the pyridine-solvated complex $FeTPP(py)_2\cdot 2py$.[18]

Table VI. d-Electron Orbital Populations (Percentages in Parentheses)

	exptl			
orbital	cryst 1	cryst 2	theoretical	spherical
$d_{x^2-y^2}$	0.57 (8.4)	0.35 (4.8)	0.81 (11.0)	1.2 (20)
d_{z^2}	0.83 (12.2)	1.05 (14.4)	0.724 (9.8)	1.2 (20)
d_{xz}	1.78 (26.1)	1.93 (26.5)	1.93 (26.1)	1.2 (20)
d_{yz}	1.78 (26.1)	1.93 (26.5)	1.93 (26.1)	1.2 (20)
d_{xy}	1.86 (27.3)	2.02 (27.7)	1.99 (27.0)	1.2 (20)
total	6.82	7.29	7.40	6.00

The shortness of the axial Fe–N_3 distance in both structures is related to the relatively large values (43.12 (6) and 34.4°) of the dihedral angle ϕ between the coordinate plane containing the opposite pyrrole nitrogen atoms and the axial ligand plane.[19] It has been shown that this angle is sensitive to the packing of the molecules in the crystal; small values are associated with longer axial bond lengths and higher spin multiplicity of the ground-state configuration.[19] There is no indication, however, that the relatively small change from 43.1 to 34.4° has such an effect.

As the iron atom is located on a center of symmetry, it lies exactly in the plane of the porphyrin ring. The dihedral angle between the porphyrin plane and the plane of the axial pyridine ligand is 74.74 (3)°, the Fe–N_3 bond being displaced from the normal of the porphyrin plane by about 7°. The angles between the porphyrin plane and the planes of the two independent phenyl groups are 74.05 (3)° for the C_{11}–C_{16} and 60.72 (2)° for the C_{17}–C_{22} phenyl groups, respectively. The plane equations and distances from the porphyrin, pyridine, and phenyl planes are given in the supplementary material.

Deformation Maps. Deformation density maps (Figures 5–7) have been calculated with data of $(\sin\theta)/\lambda < 0.7$ Å^{-1} and atomic parameters from the multipole refinements. They show density in the directions bisecting the iron–pyrrole nitrogen bonds, as may be expected for a low-spin complex with preferential occupancy of the d_{xy} orbital. Bonding density is observed in all C–C and C–N bonds. The peaks in C_β–C_β and C_β–C_α are located slightly outside the pyrrole ring, indicating strain in the five-membered ring as found in other porphyrin compounds.[6,7] The peaks in the C_β–C_β bonds are higher than those in other pyrrole bonds, indicating a larger double-bond character of this peripheral bond.

Figure 6 shows the electron density distribution in the pyridine plane for both crystals. The relative height of the bond peaks suggests a quinoid contribution to the electronic state of the pyridine ligand.

Deformation density distribution maps in sections perpendicular to the porphyrin plane are shown in Figure 7. They show electron accumulation in the crystal field stabilized orbitals, d_{xz} and d_{yz}. The maps for crystals 1 and 2 are very similar, though there is a tendency for the peak heights in the former to be lower, especially in the region around the iron atom. This indicates that the 0.91-Å^{-1} cutoff for crystal 1 is not completely adequate for the determination of iron atomic parameters unbiased by bonding asphericity.

Atomic Multipole Populations. The atomic multipole populations are listed in the supplementary material. The negative values of P_{40} for the iron atom indicate a deficiency of electron density along the z axis, relative to the spherical atom. Similarly, the negative value of P_{44+} indicates electron withdrawal from the x and y axis directions, in agreement with the features in Figure 5.

The valence electron population of iron is 7.29, corresponding to a net donation of 1.29 electrons to the Fe^{2+} ion from the ligands. All nitrogen atoms bear negative charges, the pyrrole nitrogens being more negative (−0.45 (8) electron) than the pyridine nitrogen atom (−0.23(11) electron). The total charge on the pyridine ligand is −0.37 (12) electron. Thus, the π-back-donation from the metal to the axial ligand more than balances the effects of σ-donation.

d-Electron Populations from the Multipole Parameters. The populations of the d orbitals may be derived from the multipole

(18) Li, N.; Petricek, V.; Coppens, P.; Landrum, J. *Acta Crystallogr., Sect. C: Cryst. Struct. Commun.* **1985**, *C41*, 902–905.

(19) Scheidt, W. R.; Young, Ja Lee. *Struct. Bonding (Berlin)*, in press.

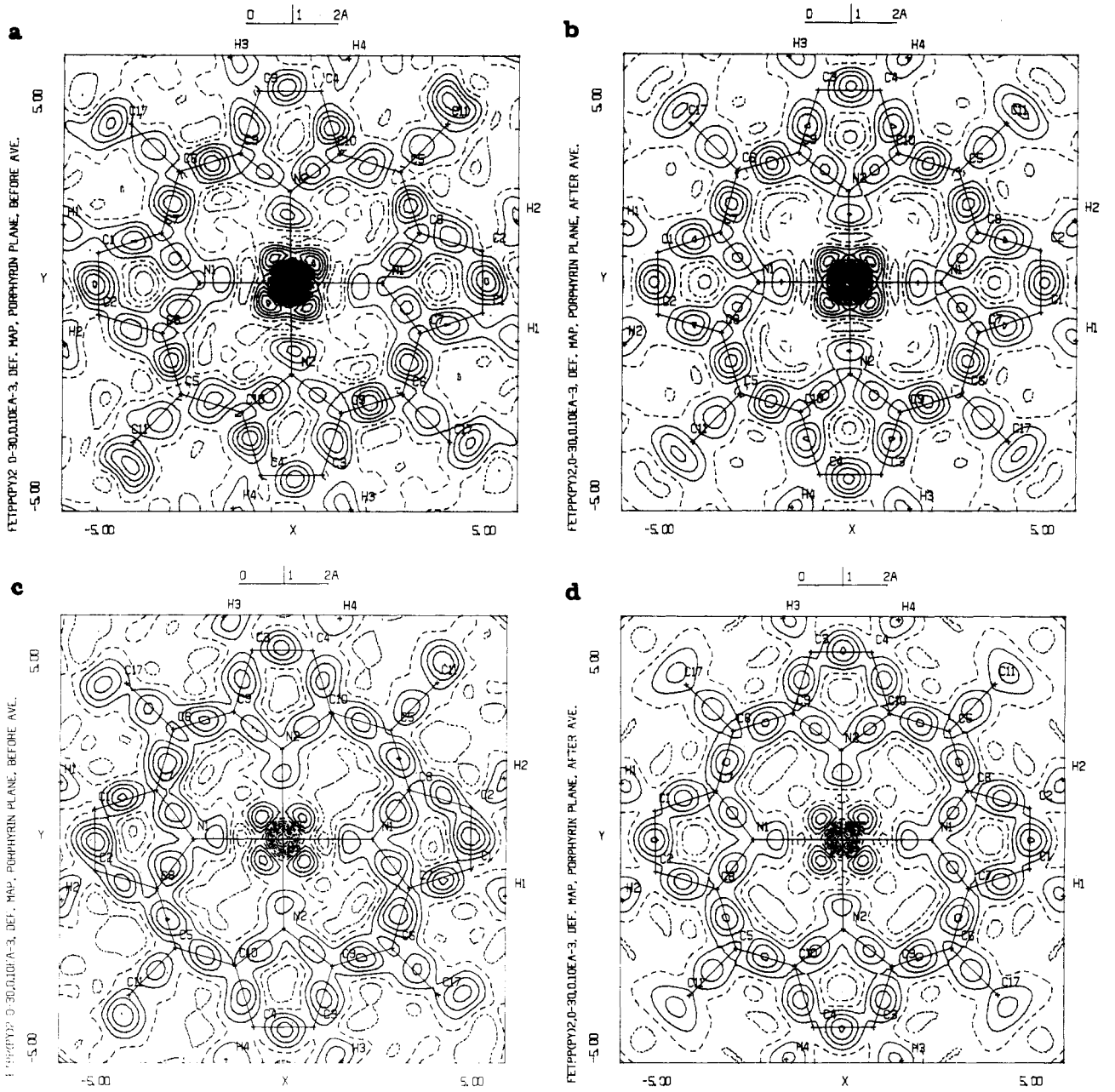

Figure 5. Deformation densities in the porphyrin plane: (a) crystal 2, before averaging; (b) crystal 2, after averaging; (c) as (a) but for crystal 1; (d) as (b) but for crystal 1. All contours are as in Figure 4.

results, as described previously.[20a] They are compared with results from an extended Hückel calculation[20b] in Table VI. There is good agreement with the theoretical populations, except for the $d_{x^2-y^2}$ orbital, the population of which seems to be overestimated in the Hückel calculation, which predicts the population of $d_{x^2-y^2}$ to be larger than that of d_{z^2}, in disagreement with experiment. About 80% of the electrons are in the crystal field stabilized d_{xy}, d_{xz}, and d_{yz} orbitals, which would contain all the electrons in a crystal field description.

The population of the $d_{x^2-y^2}$ orbital may be compared with corresponding numbers for iron(II) phthalocyanine (FePc) and iron(II) tetraphenylporphyrin (FeTPP) (Table VII), in which these orbitals are also populated due to σ-donation from the ligands. The iron–nitrogen bond length is shortest in FePc, which also has the largest population. Comparison of the three sets of results show a correlation between bond length and orbital population (Table VII).

Table VII. Comparison of $d_{x^2-y^2}$ Orbital Populations and Covalency Parameters

	S	pop. [%]	Fe–N bond length, Å	covalency parameter γ	ref
FePc	1	0.70 (7) [12.9]	1.928 (1)	0.74	6
FeTPP	1	0.43 (13) [6]	1.967 (2)	0.52	7
$FeTPP(py)_2$	0	0.35 (7) [4.8]	2.001 (1)	0.46	this work

The populations may be used directly to calculate the covalency parameter γ, defined by the expression for the bonding orbital

$$\psi = N_\sigma(\gamma d_{x^2-y^2} + \chi)$$

where χ is a linear combination of ligand s and p orbitals.[21] For the doubly occupied bonding orbital we obtain

$$\rho = 2\frac{\gamma^2 d^2 + \chi^2 + 2\gamma\chi d}{1 + 2\gamma S + \gamma^2}$$

(20) (a) Holladay, A.; Leung, P. C.; Coppens, P. *Acta Crystallogr., Sect. A: Found. Crystallogr.* **1983**, *A39*, 377–387. (b) Scheidt, W. R., private communication.

(21) Coppens, P.; Koritsanszky, T.; Becker, P. *Chem. Scr.* **1986**, *26*, 463–467.

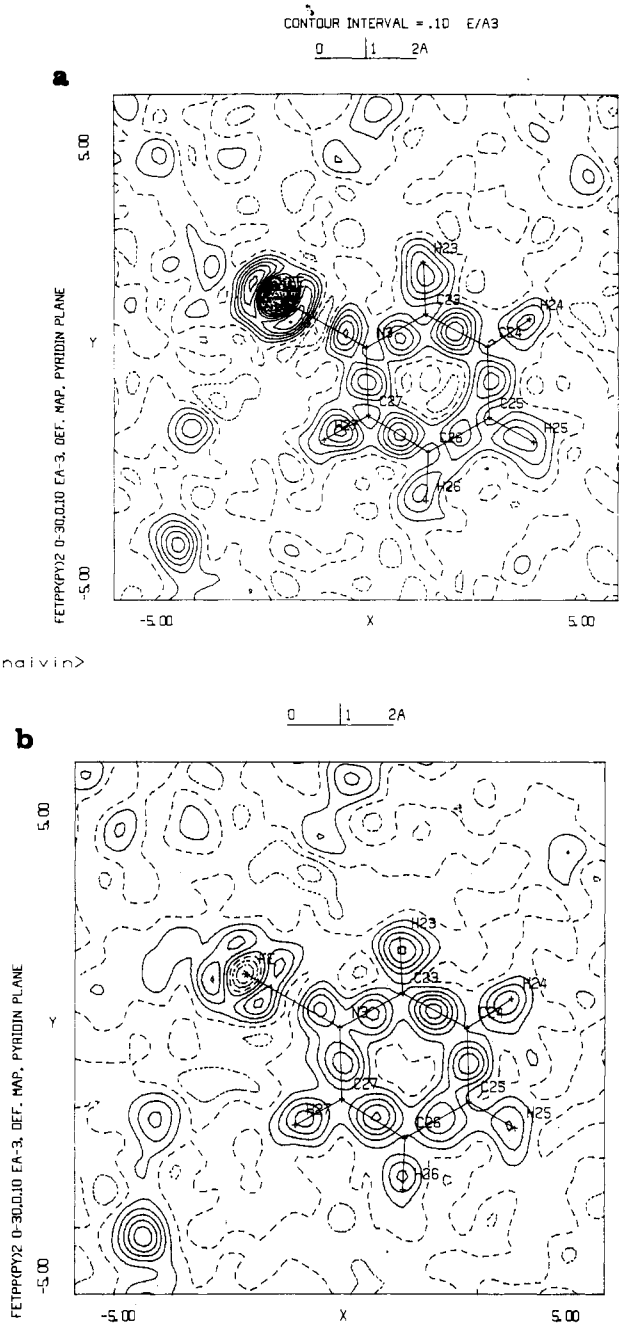

Figure 6. Deformation densities in the axial pyridine plane, with contours as in Figure 4: (a) crystal 2; (b) crystal 1.

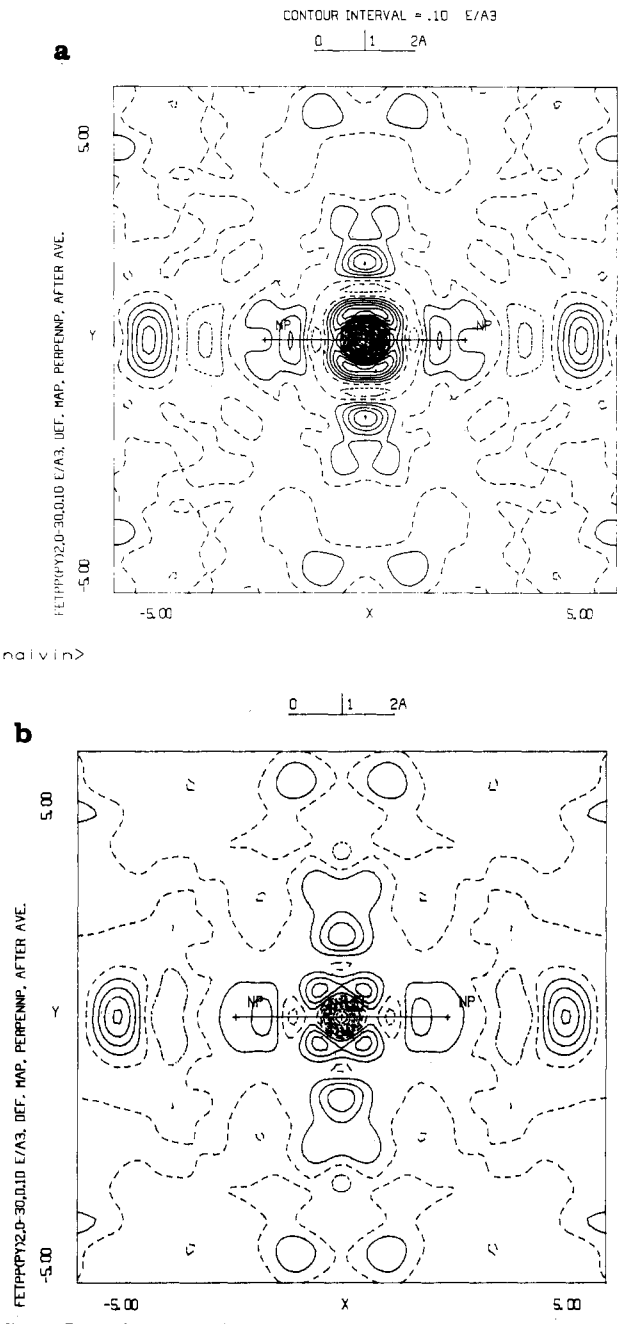

Figure 7. Deformation density maps averaged over the perpendicular sections of N_1–Fe–N_1 and N_2–Fe–N_2, with contour intervals as in Figure 4: (a) crystal 2; (b) crystal 1.

where $S = \int d_{x^2-y^2}\chi \, d\tau$. Neglecting the small overlap population, one obtains

$$\rho_{Fe} = 2\gamma^2 d^2/(1 + \gamma^2)$$

and for the d-orbital population P

$$P = 2\gamma^2/(1 + \gamma^2)$$

Substitution of the experimental P values in this equation gives γ parameters of 0.74 for FePc, 0.52 for FeTPP, and 0.46 for $FeTPP(py)_2$.

The Electric Field Gradient at the Fe Nucleus. The electric field gradient at the iron nucleus can be calculated from the populations of the multipoles.[7,22] Results may be compared with those obtained from Mössbauer resonance spectroscopy. Since the asymmetry parameter η is zero (the iron atom in $FeTPP(py)_2$ is located on a local 4-fold axis), the EFG depends only on the multipole population parameter P_{21} and the expansion–contraction parameter κ for the iron. The electric field gradients for crystals 1 and 2 are -9.6×10^{14} and -3.98×10^{15} esu/cm^2, respectively. Using the appropriate conversion factors and Sternheimer antishielding factors $\gamma = -10$ and $R_\infty = 0.22$,[23] we obtain quadrupole splittings of −0.5 (5) and −1.9 (5) mm/s for crystals 1 and 2, respectively. This result may be compared with the spectroscopic absolute value of 1.15 mm/s. Though the X-ray result is imprecise, it is in agreement with the spectroscopic value and indicates its sign to be negative.

Conclusion

This is the first electron density study of a large molecule in which two almost complete data sets have been processed independently. Comparison with previous work shows distinct differences between the electron density distributions in high-spin,

(22) Stevens, E. D.; De Lucia, M. L.; Coppens, P. *Inorg. Chem.* **1980**, *19*, 813–820.

(23) Finklea, S. L.; Cathey, L.; Amma, E. L. *Acta Crystallogr., Sect. A: Cryst. Phys., Diff., Theor. Gen. Crystallogr.* **1976**, *A32*, 529.

intermediate-spin, and low-spin complexes. While the theoretical results for the intermediate-spin complexes are controversial, remarkably good agreement with the extended Hückel results is obtained in this study, the exception being the relative ordering of the $d_{x^2-y^2}$ and d_{z^2} populations. The effect of σ-donation by the ligands is observed in all complexes studied so far. It leads to peaks along the x and y directions in the high-spin iron(II) porphyrin $FeTPP(THF)_2$ and reduces the asymmetry of the electron distribution around iron in the low-spin complex analyzed in this study.

Acknowledgment. Support of this work by the National Institutes of Health (Grant HL23884) is gratefully acknowledged. Calculations were performed in part on a VAX785 made available through a grant from the National Science Foundation (CHE8406077).

Registry No. Fe(TPP), 16591-56-3; $Fe(py)_2TPP$, 16999-25-0.

Supplementary Material Available: Figure S1, showing the definition of the local coordinate system used in the multipole refinement, and tables of maximum and minimum intensity corrections, least-squares planes, electron population parameters, hydrogen atom coordinates, and bond lengths and angles involving hydrogen atoms (16 pages); a listing of observed and calculated structure factors for crystal 2, refinement IV (51 pages). Ordering information is given on any current masthead page.

Contribution from the Departamento de Química Inorgánica-Instituto de Ciencias de Materiales, Universidad de Sevilla-CSIC, Aptdo. 553, Sevilla, Spain, Instituto de Química Inorgánica Elhúyar-Departamento de Química Inorgánica, Universidad Complutense de Madrid-CSIC, 28040 Madrid, Spain, and IPSOI, Faculté des Sciences/Saint Jérôme, UA 126 du CNRS, Université Aix-Marseille III, 13013 Marseille, France

Oxo-Molybdenum(IV) and -Tungsten(IV) Complexes with Dithio Acid Ligands. Synthesis and Structural Investigation of $MoO[S_2C(PMe_3)S\text{-}i\text{-}Pr\text{-}S,S'](S_2CS\text{-}i\text{-}Pr\text{-}S,S',C)$

Ernesto Carmona,*† Agustín Galindo,† Christian Guille-Photin,† Richard Laï,‡ Angeles Monge,§ Caridad Ruiz,§ and Luis Sánchez†

Received June 3, 1987

The title compound has been synthesized by the reaction of $MoOCl_2(PMe_3)_3$ with the potassium salt of the isopropyl thioxanthate ligand, in the presence of CS_2. The analogous reactions of the oxo complexes $MOCl_2(PMe_3)_3$ (M = Mo, W) with this and other thioxanthate ligands ^-S_2CSR (R = *i*-Pr, *t*-Bu) afford related products displaying similar IR spectral properties, but only for M = Mo and R = *i*-Pr have analytically pure crystals been isolated. The formation of the related dimethylphenylphosphine–xanthate complexes $MO[S_2C(PMe_2Ph)O\text{-}i\text{-}Pr](S_2CO\text{-}i\text{-}Pr)$ (M = Mo, W) is also reported. The molecular structure of $MoO[S_2C(PMe_3)S\text{-}i\text{-}Pr](S_2CS\text{-}i\text{-}Pr)$ has been determined by X-ray studies, which confirm that one of the thioxanthate ligands has suffered a nucleophilic attack of PMe_3 on the carbon atom of the CS_2 moiety, with formation of the zwitterionic ligand $^-S_2C^-(^+PMe_3)SR$, S,S'-bonded to the molybdenum atom, while the other acts as an η^3, S,S',C ligand. The crystals are triclinic, $P\bar{1}$, with unit cell constants a = 6.355 (3) Å, b = 12.252 (2) Å, c = 13.061 (2) Å, α = 92.96 (1)°, β = 93.65 (2)°, γ = 85.16 (3)°, and D_{calcd} = 1.61 g cm^{-3} for Z = 2. The structure was refined to an R value of 0.032 by using 3488 independent observed reflections.

Introduction

The chemistry of group 6B (6^{21}) metal complexes of dithio acid ligands has attracted considerable attention in the last few decades, in view of the possible relevance of some of these compounds to metalloenzymes, as examples of complexes with high coordination number in various oxidation states, and because of their ability to produce unique structural types of carbon- and sulfur-containing ligands, through ligand dissociation, coupling, fragmentation, or rearrangement.[1] Fruits of these studies are a very large number of complexes containing these ligands or others, thereof derived, such as thiocarboxamide, thiocarbonyl, and related groups.[2]

We have recently reported[3] that the reaction of the oxo complexes $MOCl_2(PMe_3)_3$ (M = Mo, W) with potassium *O*-alkyl xanthates KS_2COR (R = Me, Et, *i*-Pr) occurs, as in eq 1, with

$$MOCl_2(PMe_3)_3 + 2KS_2COR \xrightarrow{THF} MO[S_2C(PMe_3)OR](S_2COR) + 2PMe_3 + 2KCl \quad (1)$$

formation of oxo complexes that contain two different xanthate ligands: a zwitterionic ligand, $^-S_2C^-(^+PMe_3)OR$, S,S'-bonded to the metal atom, formed by nucleophilic attack of PMe_3 on the carbon atom of the CS_2 moiety, and an η^3-S_2COR ligand, bonded through the two sulfur atoms and the carbon atom of the CS_2 group. As a continuation of these studies, we have attempted to extend the above results to related complexes of other dithio acid ligands, particularly to the thioxanthate ligand, ^-S_2CSR. This choice was partly dictated by the previous isolation[4] of the complex $MoO(S_2CS\text{-}i\text{-}Pr)_2$, which has been shown by X-ray crystallography to contain a thioxanthate group exhibiting the usual bidentate geometry and a second acting as a nonclassical η^3 S,S',C ligand, and by the isolation of its PPh_3 adduct, $MoO(S_2CS\text{-}i\text{-}Pr)_2(PPh_3)$, from the reaction of the dinuclear complex $Mo_2O_3(S_2CS\text{-}i\text{-}Pr)_4$ with an excess of PPh_3.[4] In this paper, we report the synthesis of the new dithio acid complex $MoO[S_2C(PMe_3)S\text{-}i\text{-}Pr](S_2CS\text{-}i\text{-}Pr)$ and compare its structural properties, ascertained by NMR and X-ray studies, with those found for the xanthate complex analogue.[3] The ability of other phosphines to form analogous zwitterionic ligands has been demonstrated with the synthesis of the related compounds $MO[S_2C(PMe_2Ph)O\text{-}i\text{-}Pr](S_2CO\text{-}i\text{-}Pr)$ (M = Mo, W).

† Universidad Sevilla-CSIC.
‡ Universidad Complutense de Madrid-CSIC.
§ Université Aix-Marseille III.

(1) (a) Coucouvanis, D. *Prog. Inorg. Chem.* **1970**, *11*, 233. (b) Coucouvanis, D. *Prog. Inorg. Chem.* **1979**, *26*, 301. (c) Burns, R. P.; McCullough, F. P.; McAuliffe, C. A. *Adv. Inorg. Chem. Radiochem.* **1980**, *23*, 211.
(2) (a) Cotton, F. A.; Extine, M. W.; Niswander, R. H. *Inorg. Chem.* **1978**, *17*, 692. (b) Burgmayer, S. J. N.; Templeton, J. L. *Inorg. Chem.* **1985**, *24*, 3939. (c) Mayr, A.; McDermott, G. A.; Dorris, A. M.; Holder, A. K. *J. Am. Chem. Soc.* **1986**, *108*, 310. (d) Morrow, J. R.; Templeton, J. L.; Bandy, J. A.; Bannister, C.; Prout, C. K. *Inorg. Chem.* **1986**, *25*, 1923.
(3) Carmona, E.; Galindo, A.; Gutiérrez-Puebla, E.; Monge, A.; Puerta, C. *Inorg. Chem.* **1986**, *25*, 3804.
(4) Hyde, J.; Venkatasubramanian, K.; Zubieta, J. *Inorg. Chem.* **1978**, *17*, 414.
(5) Reference deleted in revision.

0020-1669/88/1327-0488$01.50/0